AIMS Mathematics, 11(1): 1900–1926.
DOI: 10.3934/math.2026079
Received: 10 October 2025
Revised: 31 December 2025
Accepted: 09 December 2025
Published: 21 January 2026

https://www.aimspress.com/journal/Math

Research article

Wright function solutions for mixed convection flow of micropolar fluid with memory effects: A Caputo fractional derivative approach

Fisal Asiri*

Department of Mathematics, Taibah University, Medina, 42353, Saudi Arabia.

* **Correspondence:** Email: fahasiri@taibahu.edu.sa.

Abstract: This investigation systematically examined mixed convection flow of a fractional micropolar fluid over an oscillating plate, incorporating thermal radiation and memory effects through Caputo fractional derivatives. The governing equations of the proposed problem were non-dimensionalized using appropriate dimensionless variables. Exact solutions for velocity, microrotation, and temperature distributions were derived via the Laplace transform method. The obtained exact solutions were expressed in terms of Wright functions to preserve memory characteristics. Special cases, including Stokes' first problem and fractional viscous fluids, were demonstrated, which showed the model's versatility. The influences of key parameters, such as fractional order (α), micropolar material parameter (β), Grashof number (Gr), Prandtl number (Pr), and radiation parameter (R) on flow and heat transfer characteristics, were analyzed and presented in various graphs. Graphical results illustrate parametric trends emphasizing memory effects, while tabulated data quantified skin friction, wall couple stress, and Nusselt number variations. The results yielded: (1) a generalized fractional micropolar model capturing memory effects, (2) new insights into radiation's role in thermal boundary layer modulation under non-local dynamics, and (3) benchmark solutions for microfluidic device design. This work unified fractional calculus (with its inherent memory effects), micropolar theory, and oscillatory boundary conditions, establishing a foundation for advanced fluid mechanics research.

Keywords: heat transfer, micropolar fluid; oscillating boundary; exact solutions; integral transform
Mathematics Subject Classification: Primary: 35R11; Secondary: 76E06, 44A10, 80A20, 76D05

1. Introduction

Niels Abel's 1823 approach to the autochrome phenomenon was its first application in practice in solving integral problems, while its conceptual roots remain similar to those of traditional calculus, with Euler and Fourier considering arbitrary-order derivatives. Although the area was mostly restricted to theoretical mathematics for over a century, Liouville later offered the first demanding mathematical description of fractional derivatives [1], but in the latter part of the 20th and early 21st centuries, a paradigm change occurred when fractional calculus emerged as an effective instrument for describing intricate real-world phenomena that are marked by power-law dynamics, memory effects, and non-locality. Fractional calculus is now a very useful tool in many different domains, having advanced far beyond abstract theory. In fields such as fluid mechanics [2], where it aids in the modeling of complex flows; bioengineering [3], where it simulates tissue behavior and drug delivery; electrochemistry [4], where it enhances battery models and reaction kinetics; signal processing [5], which facilitates better analysis of real-world data; and viscoelasticity [6], where it captures the memory-dependent behavior of polymers and gels, researchers now frequently use it. Fractional models are particularly useful in fluid dynamics for investigating non-Newtonian fluids, such as blood, creams, or molten polymers, since they provide more precise predictions of their flow behavior, heat transfer, and small-scale interactions than conventional techniques. New applications in fields like anomalous diffusion [7] (e.g., pollutant dispersion or cellular transport), thermodynamic modeling of memory-dependent materials [8] (e.g., shape-memory alloys), and data-driven parameter identification [9] in complex systems using machine learning are just a few examples of recent expansions that continue to increase its utility. This continuous development demonstrates how fractional calculus has genuinely transformed from a mathematical curiosity into a versatile, crucial foundation for contemporary engineering and research.

In the meantime, a significant departure from traditional modeling techniques is represented by the creation of fractional derivative models for fluids, both Newtonian and non-Newtonian. In contrast to conventional techniques, these models more correctly depict how fluids "remember" previous loads and deformations by capturing subtle fluid behaviors such as memory effects and genetic characteristics. This is particularly helpful for comprehending and forecasting the behavior of complicated fluids under real-world circumstances, such as blood, polymer solutions, or colloidal suspensions. These generalized models are obtained by methodically substituting fractional-order operators for the typical time derivatives in traditional constitutive equations. This allows the fluid's stress-strain relationship to incorporate non-locality and long-range temporal dependencies. For instance, well-established non-Newtonian frameworks, including the Maxwell, Oldroyd-B, and Burgers' fluid models, have been successfully extended into their fractional analogues to capture anomalous stress relaxation, frequency-dependent viscosity, and enhanced viscoelastic characteristics. Pioneering work by Friedrich [10] laid crucial groundwork by reformulating the classical Maxwell model using fractional calculus, explicitly expressing the mechanical response in terms of fractional-order relaxation and retardation times. This foundational study demonstrated that fractional operators naturally model the broad spectrum of relaxation times observed in real polymeric and biological fluids. Building on this, Tan et al.[11] analyzed unsteady channel flows of a fractional Maxwell fluid, providing early insights into the transient flow dynamics governed by fractional kinetics. Concurrently, Makris et al. [12] contributed to the field's expansion by adapting the fractional Maxwell formulation for applications in structural engineering, specifically in modeling the damping behavior of viscoelastic materials in seismic isolation devices. The research trajectory was further enriched by subsequent investigations. Zafer et al. [13] obtained analytical solutions for the velocity field in flows driven by a boundary shear stress using a fractional Maxwell formulation, while Shaikh et al. [14]

explored the hydrodynamic start-up flow of a fractional Oldroyd-B fluid within an annular geometry, highlighting the interplay between fractional parameters. Together, these and numerous additional studies [15–17] have established a solid mathematical and practical basis for the use of fractional calculus in rheology. They unambiguously demonstrate that fractional models perform better than conventional methods in forecasting the behavior of complicated fluids, including synthetic polymers, molten plastics, biological fluids like blood or mucus, and even geophysical materials like sediment or magma. This expanding quantity of work demonstrates the profound impact of fractional calculus. It is more than simply a theoretical update; it is strengthening our basic comprehension of fluid behavior and significantly increasing our capacity to simulate and forecast fluid occurrences in the real world.

Tan et al. [18] made a significant breakthrough by adding fractional derivatives to the constitutive model of a second-grade fluid, building on previous fundamental work on fractional viscoelastic fluids. Because of this change, the model was able to account for hereditary effects, which means that the fluid's current behavior is now influenced by its history of deformation rather than just its current condition. Compared to conventional models, this method provides a deeper and more physically realistic depiction of the natural memory-dependent response observed in many non-Newtonian fluids, such as biological materials or polymer solutions. By deriving exact analytical solutions for oscillating flows of a generalized Casson fluid, Khan et al. [19] expanded on this strategy and showed how fractional calculus may accurately represent the variable shear-thinning tendency under motion that is periodic. Subsequently, Kamran et al. [20] analyzed unsteady rotational flow of a fractional second-grade fluid through a circular cylinder, highlighting the influence of fractional parameters on torque and angular velocity. A critical limitation of these studies, however, was their exclusive focus on momentum transfer, neglecting the coupled thermal dynamics that often govern real-world applications. Recognizing this gap, Shakeel et al. [21] pioneered the extension of time-fractional derivatives to heat transfer phenomena, investigating free convection flow of a viscous fluid near a vertical plate and uncovering memory effects in thermal boundary layer development. This thematic progression continued with Khan et al. [22], who integrated the Caputo fractional derivative into the constitutive equation of a generalized Casson fluid flowing over an infinite oscillating plate, thereby coupling non-integer order dynamics with wall-driven motion. Shah and Khan [23] expanded this framework by employing the Caputo-Fabrizio derivative, notable for its non-singular kernel, to study heat transfer in a second-grade fluid over an oscillating plate, revealing enhanced accuracy in modeling thermal memory. Furthermore, Ali et al. [24] obtained exact solutions involving special functions for free convective heat transfer in a generalized Brinkman-type fluid, underscoring the analytical tractability of fractional models even with coupled heat flow. The application of fractional calculus extends to numerous non-Newtonian fluid models, offering a superior framework for capturing their memory-dependent and hereditary properties in thermal and solute transport processes [25–27]. Within this class of fluids, the micropolar model is particularly notable for its ability to describe fluids containing microstructures, such as polymeric suspensions or liquid crystals. This study, therefore, focuses on implementing a fractional derivative formulation to investigate combined heat and mass transfer within a micropolar fluid flow.

Micropolar fluids represent a fundamental subclass of microfluids characterized by six independent degrees of freedom: three for translational motion and three for rotational motion. This advanced constitutive framework accounts not only for classical velocity fields but also for microrotation, a local internal rotation of fluid particles, and micro-rotational inertia, enabling the modeling of fluids with inherent microstructure such as liquid crystals, colloidal suspensions, polymeric fluids, biological fluids, and lubricants containing suspended particles. The foundational theory for these fluids was first established by Eringen [28], who introduced the broad concept of

microfluids and systematically categorized them into three distinct classes based on their kinematic and microstructural properties. Ariman and Cakmak [29] made early theoretical advances by creating some of the earliest analytical solutions for basic micropolar fluid flows. Their research highlighted the significance of micro-rotational effects and helped to explain how these fluids behave differently from conventional Newtonian fluids. The effects of magnetic fields on micropolar fluids flowing across a moving surface were further investigated by Seddeek et al. [30]. They demonstrated how magnetic forces, also known as Lorentz forces, impact the fluid's internal rotation, or microrotation, in addition to its velocity, exposing more intricate physical layers. Further developments resulted from the search for precise answers under time-dependent circumstances. For instance, unsteady flows close to an oscillating plate where fluid motion is driven by both temperature and concentration variations were examined by Sharief et al. [31] and Khalid et al. [32]. Their research shedes significant light on the interactions between heat, mass, and microstructure in dynamic systems, both mathematically and physically. By creating exact solutions for heat and mass transfer in micropolar fluids under Newtonian heating conditions, Hussanan et al. [33] achieved significant progress. Their research provided a more comprehensive understanding of the interrelationships between temperature, concentration, and the fluid's internal micro-rotation. By examining real-world situations such as flow through porous materials, peristaltic pumping (seen in biological systems), and boundary layer behavior, other studies [34–36] have further increased the applicability of micropolar models. These studies attest to the adaptability and applicability of micropolar theory in a variety of real-world situations. The incorporation of fractional calculus into micropolar fluid dynamics, particularly for flows with oscillatory boundaries and memory-dependent heat and mass transport, is yet an unexplored field. In the end, closing this gap could boost theoretical and applied research in the field by enabling more effective and predictive models that include history-dependent effects frequently observed in complex fluids like polymers, biological media, or smart materials.

Based on the discussed literature, we came to know that fractional operators have been successfully applied to various fluid models, yet their application to micropolar fluid systems, essential for describing fluids with suspended microstructures, remains entirely unexplored. To address these research gaps, the major contributions and novelty of this study are as follows:

1) Develops a generalized fractional micropolar fluid model that simultaneously incorporates mixed convection, oscillatory boundary conditions, and thermal radiation.
2) Integrates Caputo fractional derivatives to realistically capture thermal and momentum memory effects, which are absent in classical micropolar models.
3) Derives exact analytical solutions for velocity, microrotation, and temperature fields using the Laplace transform technique, expressed in terms of Wright functions.
4) Demonstrates the versatility of the proposed model by recovering important limiting cases, including Stokes' first problem and fractional viscous fluids.
5) Provides benchmark analytical results for skin friction, wall couple stress, and Nusselt number, useful for validation of numerical and experimental studies.
6) Offers new physical insights into how thermal radiation interacts with nonlocal (fractional) dynamics in modulating the thermal boundary layer.

In light of the above discussion, the following research questions are formulated to guide this study.

1) How do fractional-order derivatives influence velocity, microrotation, and temperature distributions in mixed convection micropolar flows?
2) What is the role of thermal radiation in altering heat transfer characteristics under memory-dependent fluid behavior?

3) How do key parameters such as α, β, Gr, Pr, R affect flow, skin friction, wall couple stress, Nusselt number, and thermal responses?
4) How can the obtained exact solutions serve as reliable benchmarks for the design and analysis of microfluidic and thermal systems?

2. Description of the problem

This study analyzes an unsteady, one-dimensional free convection flow of an incompressible micropolar fluid past an infinite vertical plate. The physical configuration, illustrated in Figure 1, consists of a rigid plate that is set into oscillatory motion in its own plane at time $t = 0$. The definition of a Cartesian coordinate framework is that the x-axis is aligned to the gravitational field and the direction of plate motion, whereas the y-axis is normal to the plate surface. At a fixed temperature T_∞, the fluid is initially stationary and isothermal. The oscillation of the plate ($u(0,t) = UH(t)\cos\omega t$) starts the motion at $t = 0^+$. At the same time, a buoyancy force is created by instantly raising the plate temperature to a constant value T_w, which is maintained for all $t > 0$.

Assuming the flow is unidirectional and applying the Boussinesq approximation, the governing equations for momentum, microrotation, and energy are derived as follows [32,37]:

$$\rho\frac{\partial u(y,t)}{\partial t} = (\mu+\alpha_1)\frac{\partial^2 u(y,t)}{\partial y^2} + \alpha_1\frac{\partial N(y,t)}{\partial y} + g(\rho\beta_T)\left(T(y,t)-T_\infty\right); \quad y,t>0, \tag{1}$$

$$\rho j\frac{\partial N(y,t)}{\partial t} = \gamma\frac{\partial^2 N(y,t)}{\partial y^2}; \quad y,t>0, \tag{2}$$

$$\rho C_p\frac{\partial T(y,t)}{\partial t} = k_1\frac{\partial^2 T(y,t)}{\partial y^2} - \frac{\partial q_r}{\partial y}; \quad y,t>0. \tag{3}$$

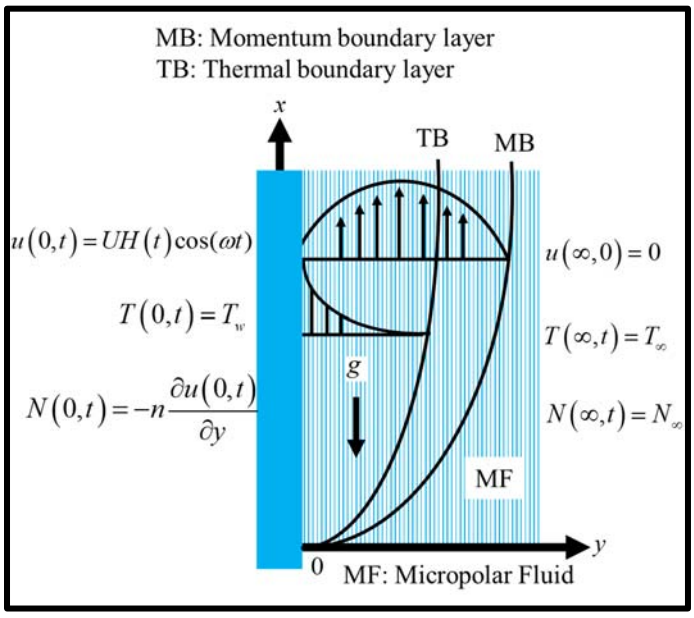

Figure 1. Geometrical sketch.

Applying the Rosseland approximation, the radiative heat flux term in Eq (3) simplifies to:

$$q_r = -\frac{4\sigma_1}{3k_2}\frac{\partial T^4}{\partial y}, \tag{4}$$

where σ_1 represents Stefan-Boltzmann constant and k_2 is the mean absorption coefficient.

By expanding T^4 using a Taylor series about the ambient temperature T_∞ and neglecting higher-order terms beyond the linear component, we obtain the linearized form as:

$$T^4 \cong 4T_\infty^3 T - 3T_\infty^4. \tag{5}$$

Substituting Eqs (4) and (5) into Eq (3) yields:

$$\rho C_p \frac{\partial T(y,t)}{\partial t} = \left(1 + \frac{16\sigma_1 T_\infty^3}{3k_1 k_2}\right)\frac{\partial^2 T(y,t)}{\partial y^2}; \quad y,t > 0. \tag{6}$$

Corresponding initial and boundary conditions are:

$$\left.\begin{array}{c} u(y,0) = 0,\ N(y,0) = 0,\ T(y,0) = T_\infty, \\ u(0,t) = UH(t)\cos\omega t,\ N(0,t) = -n\dfrac{\partial u(0,t)}{\partial y},\ T(0,t) = T_w, \\ u(\infty,t) = 0,\ N(\infty,t) = 0,\ T(\infty,t) = T_\infty \end{array}\right\}, \tag{7}$$

where $u(y,t)$ is the fluid velocity, $N(y,t)$ is the microrotation, $T(y,t)$ is the fluid temperature, ρ is the fluid density, μ is the dynamic viscosity, α_1 is the vortex viscosity, g is the gravitational acceleration, β_T is the coefficient of thermal expansion, j is microinertia, γ is spin gradient viscosity, C_p is the specific heat at constant pressure, k_1 is the thermal conductivity, q_r is radiative heat flux, U is the characteristic velocity, $H(t)$ is the Heaviside unit step function and ω is the frequency of oscillations of the plate. Introducing the nondimensional variables

$$v = \frac{u}{U}, \xi = \frac{U}{\upsilon}y,\ \tau = \frac{U^2}{\upsilon}t, N^* = \frac{\upsilon}{U^2}N,\ \ \theta = \frac{T - T_w}{T_w - T_\infty}$$

into Eqs (1), (2), (6), and (7) yields the following transformed governing equations and boundary conditions (dropping out * sign from N)

$$\frac{\partial v(\xi,\tau)}{\partial t} = (1+\beta)\frac{\partial^2 v(\xi,\tau)}{\partial \xi^2} + \beta\frac{\partial N(\xi,\tau)}{\partial \xi} + Gr\theta; \quad \xi,\ \tau > 0, \tag{8}$$

$$\frac{\partial N(\xi,\tau)}{\partial t} = \frac{1}{\eta}\frac{\partial^2 N(\xi,\tau)}{\partial \xi^2}; \quad \xi,\ \tau > 0, \tag{9}$$

$$\Pr_{eff}\frac{\partial \theta(\xi,\tau)}{\partial t} = (1+R)\frac{\partial^2 \theta(\xi,\tau)}{\partial \xi^2}; \quad \xi,\ \tau > 0, \tag{10}$$

and

$$\left.\begin{array}{c} v(\xi,0)=0,\ N(\xi,0)=0,\ \theta(\xi,0)=0, \\ v(0,\tau)=H(\tau)\cos\omega\tau,\ N(0,\tau)=-n\frac{\partial v(0,\tau)}{\partial\xi},\ \theta(0,\tau)=1, \\ v(\infty,\tau)=0,\ N(\infty,\tau)=0,\ N(\infty,\tau)=0,\ \theta(\infty,\tau)=1 \end{array}\right\}. \tag{11}$$

Here, $\beta=\frac{\alpha_1}{\mu}$ is the micropolar fluid parameter, $Gr=\frac{\upsilon g\beta_T\left(T_w-T_\infty\right)}{U^3}$ is the thermal Grashof number, $\eta=\frac{\mu j}{\gamma}$ is the dimensionless spin gradient, $\Pr=\frac{\mu C_p}{k_1}$ is the Prandtl number, $\Pr_{eff}=\frac{\Pr}{1+R}$ is the effective Prandtl number, and $R=\frac{16\sigma_1 T_\infty^3}{3k_1k_2}$ is the radiation parameter. In order to develop the generalized micropolar fluid model, the governing Eqs (7)–(9) are transformed to the Caputo time fractional model as:

$$D_t^\alpha v\left(\xi,\tau\right)=\left(1+\beta\right)\frac{\partial^2 v\left(\xi,\tau\right)}{\partial\xi^2}+\beta\frac{\partial N\left(\xi,\tau\right)}{\partial\xi}+Gr\theta;\quad \xi,\ \tau>0, \tag{12}$$

$$D_t^\alpha N=\frac{1}{\eta}\frac{\partial^2 N\left(\xi,\tau\right)}{\partial\xi^2};\quad \xi,\ \tau>0, \tag{13}$$

$$\Pr_{eff} D_t^\alpha\theta\left(\xi,\tau\right)=\left(1+R\right)\frac{\partial^2\theta\left(\xi,\tau\right)}{\partial\xi^2};\quad \xi,\ \tau>0, \tag{14}$$

where $D_t^\alpha\left(.\right)$ is the Caputo time fractional operator and is defined by [1]

$$D_t^\alpha\ f\left(t\right)=\begin{cases}\frac{1}{\Gamma\left(1-\alpha\right)}\int_0^t\frac{f'\left(\tau\right)}{\left(t-\tau\right)^\alpha}d\tau; & 0<\alpha<1, \\ \frac{\partial f(y,t)}{\partial t}; & \alpha=1.\end{cases} \tag{15}$$

3. Solutions of the problem

The set of partial differential equations (12)–(14) is solved analytically via the Laplace transform method. The solutions in the transform domain are inverted to the physical domain using a standard inverse Laplace transform technique.

3.1. Solutions for temperature profile

The Laplace transform is applied to the energy Eq (14). Utilizing the initial condition defined in (11), the transformed equation is obtained as:

$$\frac{d^2\overline{\theta}(\xi,q)}{d\xi^2}-\Pr_{eff}q^\alpha\overline{\theta}(\xi,q)=0;\quad \xi>0, \tag{16}$$

along with transformed boundary conditions:

$$\bar{\theta}(0,q)=\frac{1}{q},\ \ \bar{\theta}(\infty,q)=0. \tag{17}$$

Using Eq (17), the solution to the differential equation (16) is found to be:

$$\overline{\theta}(\xi,q)=\frac{1}{q}e^{-\xi\sqrt{\mathrm{Pr}_{eff}q^{\alpha}}}. \tag{18}$$

The solution in the physical time domain is then obtained by performing the inverse Laplace transform on Eq (18), resulting in:

$$\theta(\xi,\tau)=\Phi\left(1,-\frac{\alpha}{2};\xi\sqrt{\mathrm{Pr}_{eff}}\tau^{-\frac{\alpha}{2}}\right), \tag{19}$$

where $\Phi\left(a,b;c\right)$ is the Wright function.

3.2. Solutions for microrotation profile

The Laplace transform is applied to the momentum Eq (13). Incorporating the initial condition given by Eq (11) provides the transformed equation:

$$\frac{d^2\,\bar{N}(\xi,q)}{d\xi^2}-\eta q^{\alpha}\overline{\theta}=0;\quad \xi>0, \tag{20}$$

with transformed boundary conditions:

$$\bar{N}(0,q)=-n\frac{\partial\bar{v}\left(0,q\right)}{\partial\xi},\ \ \bar{N}(\infty,q)=0. \tag{21}$$

Employing the condition prescribed in Eq (21), the solution of Eq (20) is obtained as follows:

$$\overline{N}(\xi,q)=a_1\frac{q}{q^2+\omega^2}\sqrt{q^{\alpha}}e^{-\xi\sqrt{\eta q^{\alpha}}}+a_2\frac{1}{q\sqrt{q^{\alpha}}}e^{-\xi\sqrt{\eta q^{\alpha}}}. \tag{22}$$

The inverse Laplace transform is applied to Eq (22) to obtain the solution in the time domain:

$$N(\xi,\tau)=a_1\cos\omega\tau*\frac{1}{\tau^{\frac{\alpha}{2}+1}}\Phi\left(-\frac{\alpha}{2}-1,-\frac{\alpha}{2},-\xi\sqrt{\eta}\tau^{-\frac{\alpha}{2}}\right)+\tau^{\frac{\alpha}{2}}\Phi\left(\frac{\alpha}{2},-\frac{\alpha}{2},-\xi\sqrt{\eta}\tau^{-\frac{\alpha}{2}}\right) \tag{23}$$

where

$$a_1=\frac{n\sqrt{\beta_0}\left(\eta-\beta_0\right)}{\left(\eta-\beta_0+\eta\beta\beta_0\sqrt{\eta\beta_0}-n\beta\beta_0\eta\right)},\ a_2=a_1GrA_1-a_1nGrA_1\sqrt{\mathrm{Pr}_{eff}},\quad A_1=\frac{\beta_0}{\left(\mathrm{Pr}_{eff}-\beta_0\right)}\ and\ \beta_0=\frac{1}{1+\beta}.$$

3.3. Solutions for velocity profile

The Laplace transform is applied to Eq (12) and its associated boundary conditions are from Eq (11). Substituting the expressions from Eqs (18) and (22) into the resulting transformed equation yields:

$$\frac{d^2\bar{v}(\xi,q)}{d\xi^2}+\beta_0 q^{\alpha}\bar{v}=-\frac{d\,\bar{N}(\xi,q)}{d\xi}\pm Gr\bar{\theta},\quad \xi>0, \tag{24}$$

and

$$\bar{v}(0,q)=\frac{q}{q^2+\omega^2},\ \bar{v}(\infty,q)=0. \tag{25}$$

The solution to Eq (24), subject to the boundary conditions (25), is given by:

$$\bar{v}(\xi,q)=a_3\frac{q}{q^2+\omega^2}e^{-\xi\sqrt{\beta_0 q^{\alpha}}}+a_4\frac{q}{q^2+\omega^2}e^{-\xi\sqrt{\eta q^{\alpha}}}+\frac{a_5}{q^{\alpha+1}}e^{-\xi\sqrt{\beta_0 q^{\alpha}}}-\frac{a_6}{q^{\alpha+1}}e^{-\xi\sqrt{\eta q^{\alpha}}}-\frac{a_7}{q^{\alpha+1}}e^{-\xi\sqrt{\mathrm{Pr}_{eff}\,q^{\alpha}}}, \tag{26}$$

where

$$a_3=\left(1-a_1A_0\right),\ a_4=a_1A_0,\ a_5=GrA_1+a_2A_0,\ a_6=a_2A_0,\ a_7=GrA_1,\ A_0=\frac{\beta\beta_0\sqrt{\eta}}{\left(\eta-\beta_0\right)}.$$

Finally, applying the inverse Laplace transform to Eq (26) yields the solution for the velocity field in the time domain:

$$\begin{aligned}v(\xi,\tau)&=a_3\cos\omega\tau*\tau^{-1}\Phi\left(0,-\frac{\alpha}{2},-\xi\sqrt{\beta_0}\tau^{-\frac{\alpha}{2}}\right)+a_4\cos\omega\tau*\tau^{-1}\Phi\left(0,-\frac{\alpha}{2},-\xi\sqrt{\eta}\tau^{-\frac{\alpha}{2}}\right)\\&+a_5\tau^{-1}\Phi\left(\alpha+1,-\frac{\alpha}{2},-\xi\sqrt{\beta_0}\tau^{-\frac{\alpha}{2}}\right)-a_6\tau^{-1}\Phi\left(\alpha+1,-\frac{\alpha}{2},-\xi\sqrt{\eta}\tau^{-\frac{\alpha}{2}}\right)\\&-a_7\tau^{-1}\Phi\left(\alpha+1,-\frac{\alpha}{2},-\xi\sqrt{\mathrm{Pr}_{eff}}\tau^{-\frac{\alpha}{2}}\right).\end{aligned} \tag{27}$$

3.4. Numerical results for surface transport phenomena

The key engineering parameters, skin friction, wall couple stress, and Nusselt number, are given in their dimensional and dimensionless forms by the following expressions:

$$C_f^*=-\left(1+\frac{1}{\alpha}\right)\left.\frac{\partial u(y,t)}{\partial y}\right|_{y=0}+\alpha N\big|_{y=0}, \tag{28}$$

$$C_f=2\left[1+\left(1-n\right)\right]\left.\frac{\partial v(\xi,\tau)}{\partial\xi}\right|_{\xi=0}. \tag{29}$$

$$C_m^*=-\gamma\left.\frac{\partial N^*(y,t)}{\partial y}\right|_{y=0}, \tag{30}$$

$$C_m=-\left(1+\beta\right)\left.\frac{\partial v(\xi,\tau)}{\partial\xi}\right|_{\xi=0}. \tag{31}$$

$$\mathrm{Nu} = x\frac{\left(\frac{\partial T(y,t)}{\partial y}\right)}{T_\infty - T_w}, \tag{32}$$

$$\mathrm{Nu} = -\mathrm{Re}\frac{\partial\theta(\xi,\tau)}{\partial\xi}\bigg|_{\xi=0}. \tag{33}$$

4. Special cases

This section outlines the reduction of the generalized fractional micropolar model to several recognized fluid flow problems. These special cases serve to validate the present model, and they highlight the versatility and analytical strength of the derived solutions across different physical regimes.

4.1. Solution of Stokes' first problem

In the limiting case, when $\omega \to 0,$ the solutions obtained in Eq (27) are reduced to the form of Stokes' first problem as:

$$\begin{aligned} v(\xi,\tau) &= a_3\Phi\left(1,-\frac{\alpha}{2},-\xi\sqrt{\beta_0}\tau^{-\frac{\alpha}{2}}\right)+a_4\Phi\left(1,-\frac{\alpha}{2},-\xi\sqrt{\eta}\tau^{-\frac{\alpha}{2}}\right)\\ &+a_5\tau^{\alpha}\Phi\left(\alpha+1,-\frac{\alpha}{2},-\xi\sqrt{\beta_0}\tau^{-\frac{\alpha}{2}}\right)-a_6\tau^{\alpha}\Phi\left(\alpha+1,-\frac{\alpha}{2},-\xi\sqrt{\eta}\tau^{-\frac{\alpha}{2}}\right)\\ &-a_7\tau^{\alpha}\Phi\left(\alpha+1,-\frac{\alpha}{2},-\xi\sqrt{\beta_0}\tau^{-\frac{\alpha}{2}}\right). \end{aligned} \tag{34}$$

This confirms the consistency of our generalized model with the established theory.

4.2. Fractional viscous fluid

In the absence of micropolar effects, i.e., when the vortex viscosity parameter $\beta \to 0, \Rightarrow \beta_0 \to 1$ and Eq (27) reduce to the fractional velocity profile for a viscous (Newtonian) fluid

$$v(\xi,\tau) = \cos\omega\tau * +\tau^{-1}\Phi\left(0,-\frac{\alpha}{2},\xi\tau^{-\frac{\alpha}{2}}\right)-Gr_0\tau^{\alpha}\Phi\left(\alpha+1,-\frac{\alpha}{2},\sqrt{\mathrm{Pr}_{eff}}\xi\tau^{-\frac{\alpha}{2}}\right) \tag{35}$$

where

$$Gr_0 = \frac{Gr}{\mathrm{Pr}_{eff}-1}.$$

This recovery of the established solution validates our generalized model.

4.3. Ordinary viscous fluid

The consistency of our fractional model is verified by examining its limiting behavior. When the fractional parameter $\alpha \to 1$, the memory effects inherent to the fractional calculus vanish, and the Caputo derivative converges to the classical first-order derivative. Consequently, Eq (35) reduces to integer-order solutions.

$$\bar{v}(\xi,q)=\frac{q}{q^2+\omega^2}e^{-\xi\sqrt{q^{\alpha}}}-\frac{Gr_0}{q^2}e^{-\xi\sqrt{\Pr_{eff}\,q^{\alpha}}}, \tag{36}$$

$$\begin{aligned} v(\xi,\tau)=&\cos\left(\omega\tau-\xi\sqrt{\frac{\tau}{2}}\right)e^{-\xi\sqrt{\frac{\tau}{2}}}-\int_{\tau}^{\infty}\cos\omega(\tau-q)\frac{\xi}{2u\sqrt{\pi u}}e^{-\xi\frac{\xi^2}{4u}}du\\ &-Gr_0\left[\left(\tau+\frac{\xi^2}{2}\right)\operatorname{erf}c\left(\frac{\xi}{2\tau}\right)-\xi\sqrt{\frac{\tau}{2}}e^{-\frac{\xi^2}{4\tau}}\right]. \end{aligned} \tag{37}$$

This recovery of the classical model serves as a critical validation of our generalized fractional framework.

5. Numerical results

This section presents a comprehensive analysis of how key dimensionless parameters govern the flow behavior, thermal characteristics, and microstructural response of the fractional micropolar fluid system. The influence of dimensionless time (τ), the fractional parameter (α), micropolar material parameter (β), spin gradient viscosity (η), Grashof number (Gr), effective Prandtl number (Pr_{eff}), microgyration parameter (n), radiation parameter (R), and phase angle ($\omega\tau$) on the velocity, microrotation, and temperature profiles is systematically examined. It is important to note that the numerical values of these parameters were selected based on the studies reported in [21,24,32,37]. Particular attention is given to the distinctive memory effects introduced by the Caputo fractional derivative framework, which manifest through the fractional order α and its interaction with other physical parameters. The temperature distribution is specifically analyzed with respect to variations τ, Pr_{eff}, and R, highlighting their role in thermal boundary layer development. Each parameter's effect on the transfer of heat, fluid velocity, and rotational microstructure is demonstrated by comparative profiles for two different values. These side-by-side illustrations quantitatively show how changes in important variables impact the behavior of the system. The Wright function solutions make it possible to precisely characterize the ways in which parameters change basic flow topologies. The intricate relationship between memory effects, microstructure, and thermal transport is better understood because of this analytical method. The findings show complex relationships specific to micropolar fluid systems.

Figures 2–12 illustrate the influence of the fractional order parameter α on the velocity, microrotation, and temperature profiles. These figures reveal that all three profiles increase monotonically with increasing values of α and attain their maximum magnitudes at $\alpha=1$, which corresponds to the classical integer-order case. In contrast, for $\alpha<1$, the profiles exhibit noticeably reduced magnitudes, reflecting the strong memory effect inherent in the fractional-order formulation. This memory effect accounts for the history-dependent behavior of the fluid, leading to delayed momentum and thermal diffusion compared to the classical model.

The memory effects observed for $\alpha<1$ are particularly relevant to polymeric fluids, where molecular chain entanglement causes stress relaxation and delayed deformation under applied forces. Similarly, in biological fluids such as blood, synovial fluid, and cytoplasmic flows, the presence of suspended cells and micro-constituents induces history-dependent rheological behavior, which is effectively captured by fractional-order micropolar models. Moreover, materials with hereditary properties, including viscoelastic composites and smart materials, exhibit responses that depend on past loading conditions. In such systems, the fractional-order formulation combined with micropolar effects provides a more realistic representation of momentum and thermal transport mechanisms than

classical integer-order models.

The influence of dimensionless time (τ) on flow behavior is shown in Figure 2(a), (b). Velocity profiles rise significantly with increasing τ . This occurs due to enhanced momentum diffusion from the oscillating plate. Fluid particles gain kinetic energy over time, accelerating the flow. Microrotation intensity also grows with time. Longer duration allows stronger transmission of rotational effects. Shear from the boundary progressively excites microstructural rotation.

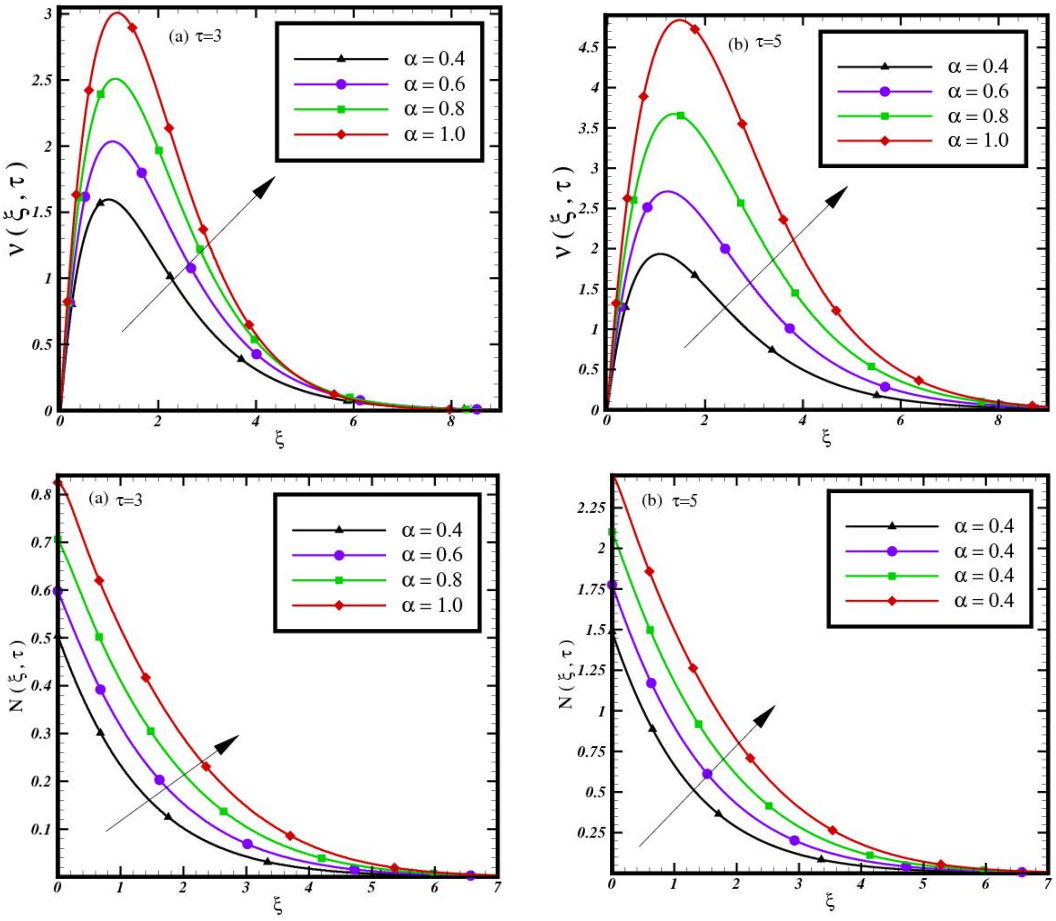

Figure 2. Velocity and microrotation profiles against ξ for different values of τ *(a)* $\tau=3$ and *(b)* $\tau=5$, where $\beta=0.2$, $\eta=1.5$, $Gr=10$, Pr=10, $n=0.1$, $R=2$, and $\omega\tau=\pi/2$.

Figure 3(a),(b) illustrates the influence of the micropolar parameter β on velocity and microrotation profiles. These figures clearly demonstrate that β exerts a suppressing effect on both flow fields. Specifically, velocity and microrotation magnitudes decrease consistently as β increases. This phenomenon has a clear physical interpretation. The parameter β represents the ratio of vortex viscosity to shear viscosity. Higher β values indicate stronger microstructural resistance to fluid motion. Consequently, this resistance reduces both translational and rotational momentum within the fluid. Furthermore, the enhanced viscous effects thicken the momentum boundary layer. This thickening reduces velocity gradients near the boundary. Meanwhile, the fluid's internal resistance to rotation increases significantly. This dual effect explains the observed suppression of both hydrodynamic characteristics.

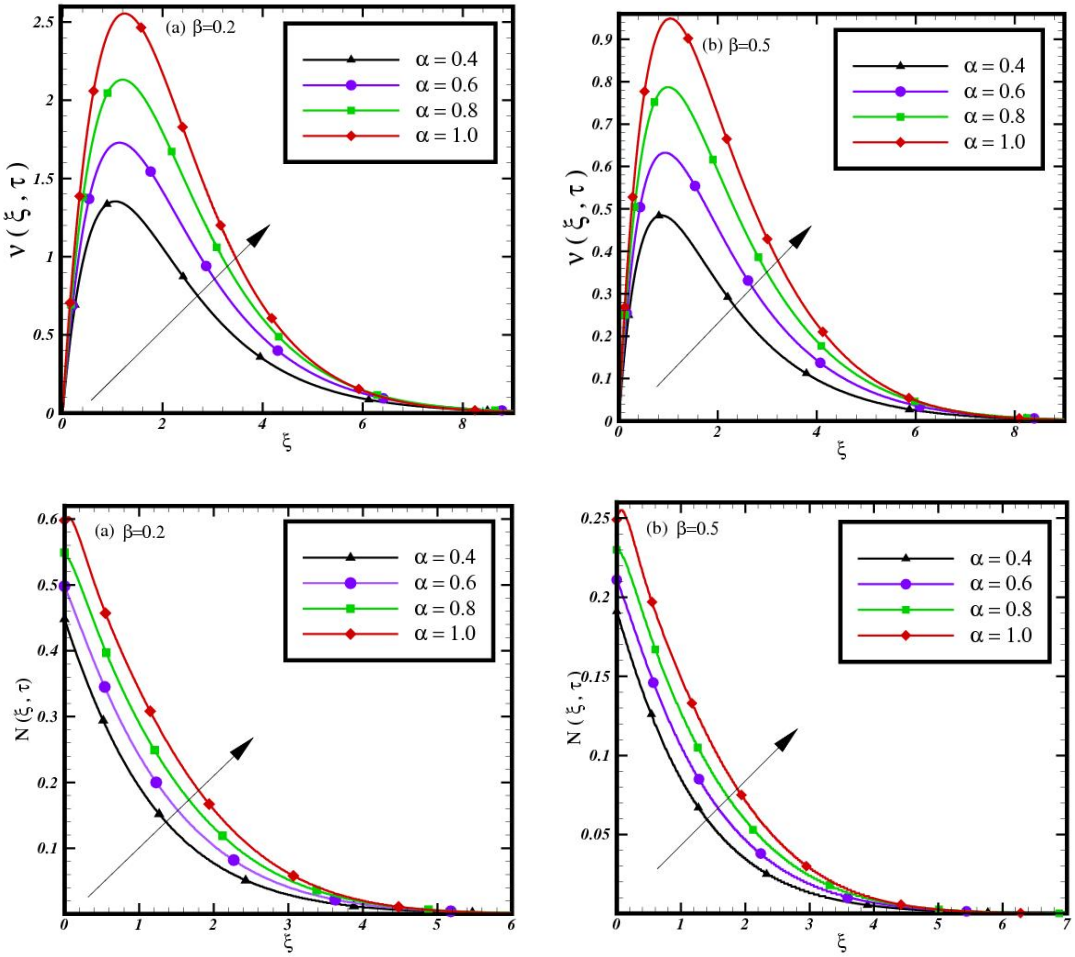

Figure 3. Velocity and microrotation profiles against ξ for different values of β (a) $\beta=0.2$ and (b) $\beta=0.5$ where $\tau=3$, $\eta=1.5$, $Gr=10$, $\mathrm{Pr}=10$, $n=0.1$, $R=2$, and $\omega\tau=\pi/2$.

Figure 4(a),(b) displays the effect of spin gradient viscosity (η) on velocity and microrotation. Velocity profiles show a clear increase with higher values of η. This occurs because enhanced spin gradient viscosity improves momentum transfer. Meanwhile, microrotation demonstrates a decreasing trend under the same conditions. This opposing behavior reflects the competitive energy distribution in micropolar fluids. Higher η facilitates better diffusion of rotational momentum. Consequently, this reduces local angular velocity gradients. At the same time, it promotes translational kinetic energy. Thus, the fluid experiences lower resistance to bulk flow. In addition, the thickened momentum boundary layer supports faster movement. However, rotational effects become more dispersed and less intense.

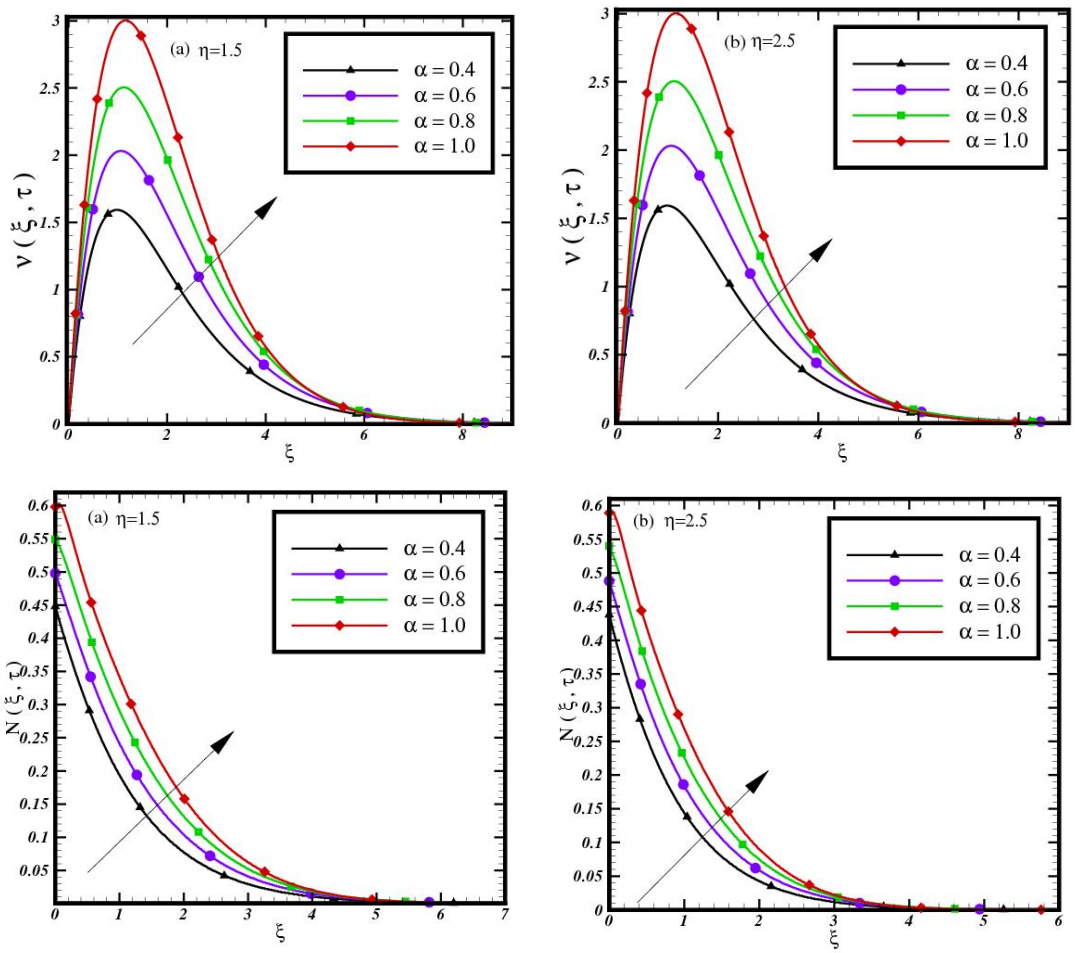

Figure 4. Velocity and microrotation profiles against ξ for different values of η (a) $\eta=1.5$ and (b) $\eta=2.5$, where $\tau=3$, $\beta=0.2$, $Gr=10$, Pr$=10$, $n=0.1$, $R=2$, and $\omega\tau=\pi/2$.

Figure 5(a),(b) demonstrates the influence of the Gr on velocity and microrotation profiles. Increasing Gr enhances both velocity and microrotation magnitudes significantly. This trend occurs due to strengthened thermal buoyancy effects. A higher Gr value indicates dominant buoyancy forces over viscous forces. This thickens the thermal boundary layer and intensifies temperature gradients. Consequently, the enhanced buoyancy drives stronger convective fluid motion. Meanwhile, the increased fluid circulation generates greater vorticity. This elevated shear rate subsequently excites microrotation. Furthermore, the microstructure responds more actively to stronger thermal forcing. Thus, both translational and rotational motions are amplified. In addition, the fractional model captures memory effects from past thermal states. This leads to sustained acceleration compared to classical approaches. Understanding Gr is vital for thermally driven micropolar flows.

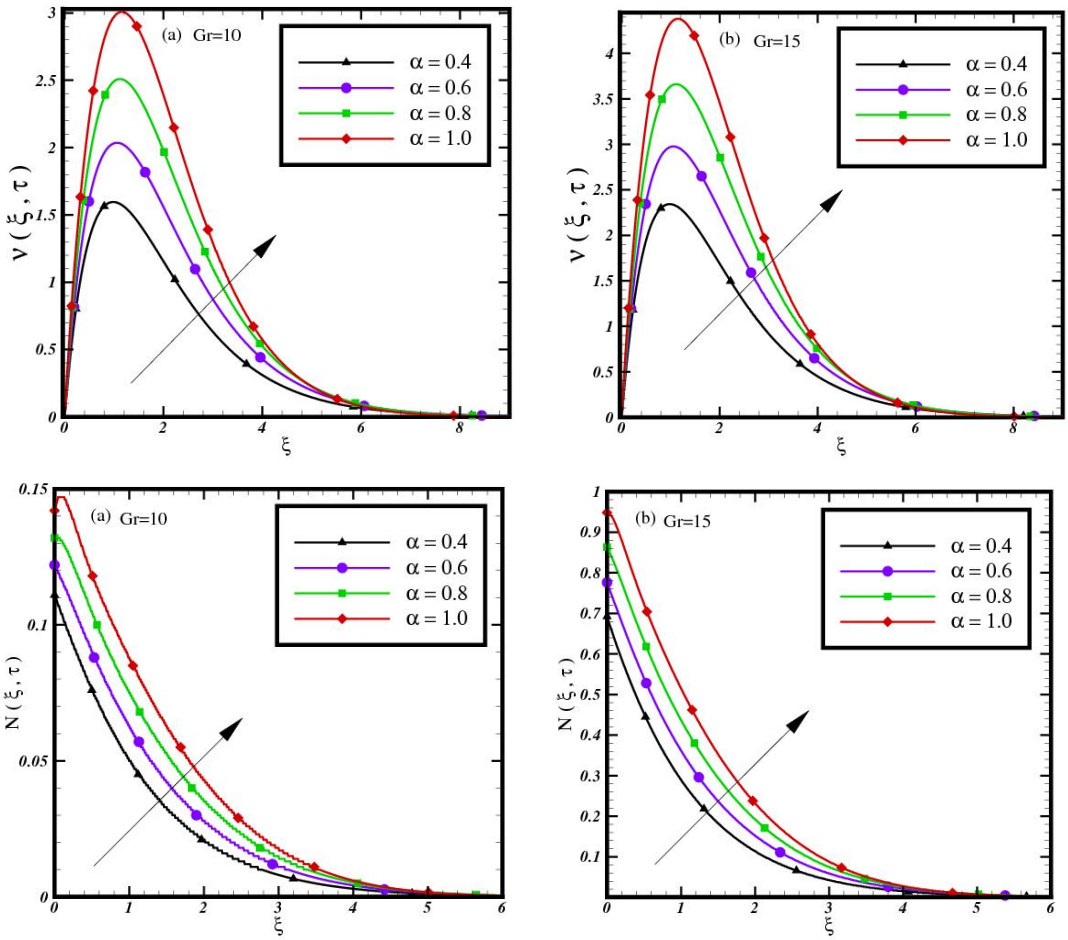

Figure 5. Velocity and microrotation profiles against ξ for different values of *Gr* (a) *Gr=10* and (b) *Gr=15, where τ=3, β=0.2, η=1.5,* Pr*=10, n=0.1, R=2,* and *ωτ=π/2.*

Figure 6(a), (b) depicts the influence of the Pr_{eff} on velocity and microrotation. Both flow characteristics show a decreasing trend as Pr_{eff} increases. This behavior results from altered thermal and momentum transport properties. Higher Pr_{eff} values indicate reduced thermal diffusivity relative to momentum diffusivity. This reduces thermal boundary layer thickness significantly. Meanwhile, the momentum boundary layer remains less affected by this change. Consequently, temperature gradients near the wall become steeper. This intensifies heat conduction effects locally. Meanwhile, viscous forces become increasingly dominant in the flow domain. The stronger viscous effects resist fluid motion more effectively. Thus, velocity profiles show reduced magnitudes overall. Additionally, diminished flow energy provides less excitation for microrotation. Furthermore, the suppressed convection limits rotational activation. In addition, the fractional model captures how memory effects interact with this suppression. This leads to a sustained reduction in both kinematic fields.

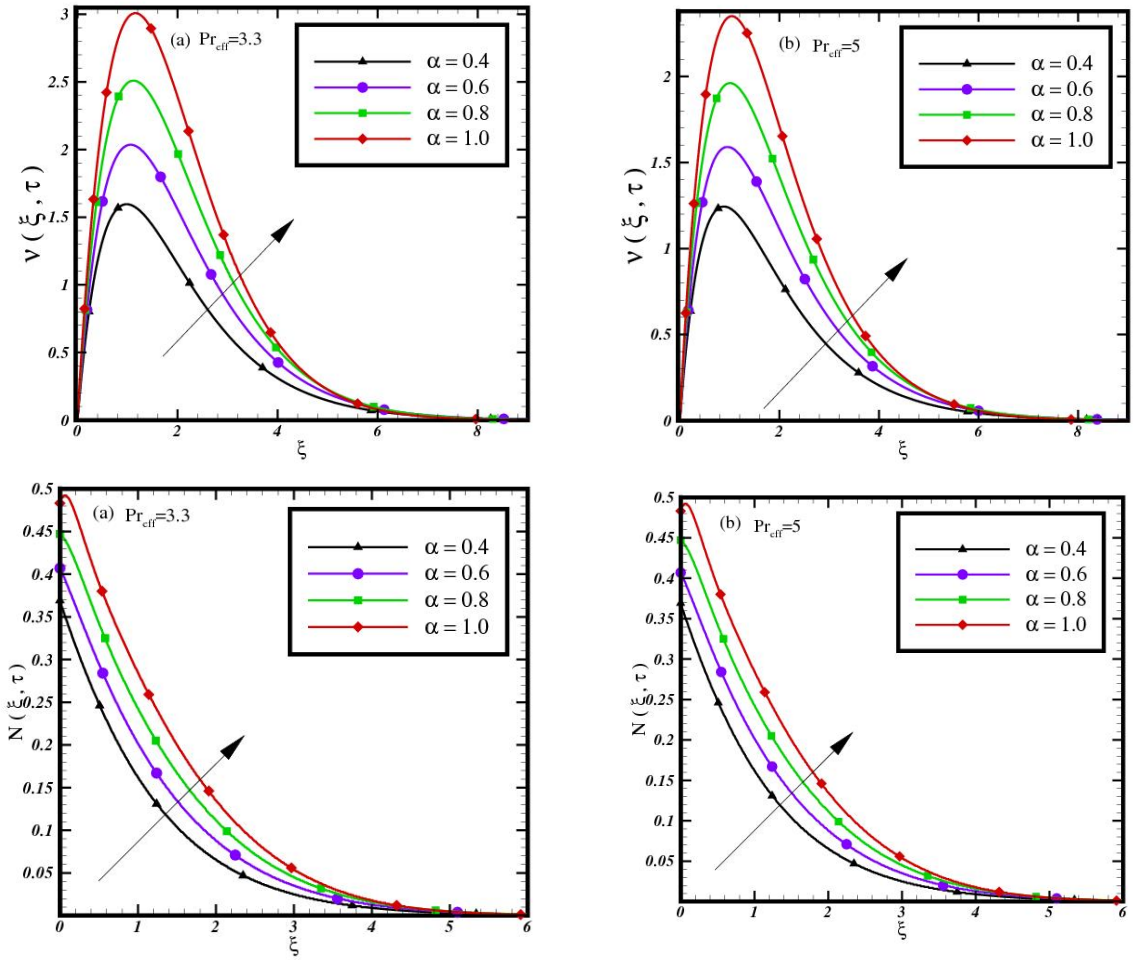

Figure 6. Velocity and microrotation profiles against ξ for different values of Pr_{eff} (a) Pr_{eff} =3.3 and (b) Pr_{eff} =*5*, where τ*=3,* β*=0.2,* η*=1.5, Gr=10,* Pr*=10, n=0.1, R=2,* and $\omega\tau=\pi/2$.

Figure 7(a),(b) illustrates the effect of the parameter n on velocity and microrotation. As n increases, the velocity amplitude decreases significantly, while the microrotation distribution shows substantial enhancement. This contrasting behavior arises from energy redistribution between translational and rotational motion. Higher n values strengthen the coupling between velocity and microrotation, transferring more energy to rotational degrees of freedom and leaving less for translational motion. The intensified microrotation also increases flow resistance, further suppressing the velocity field.

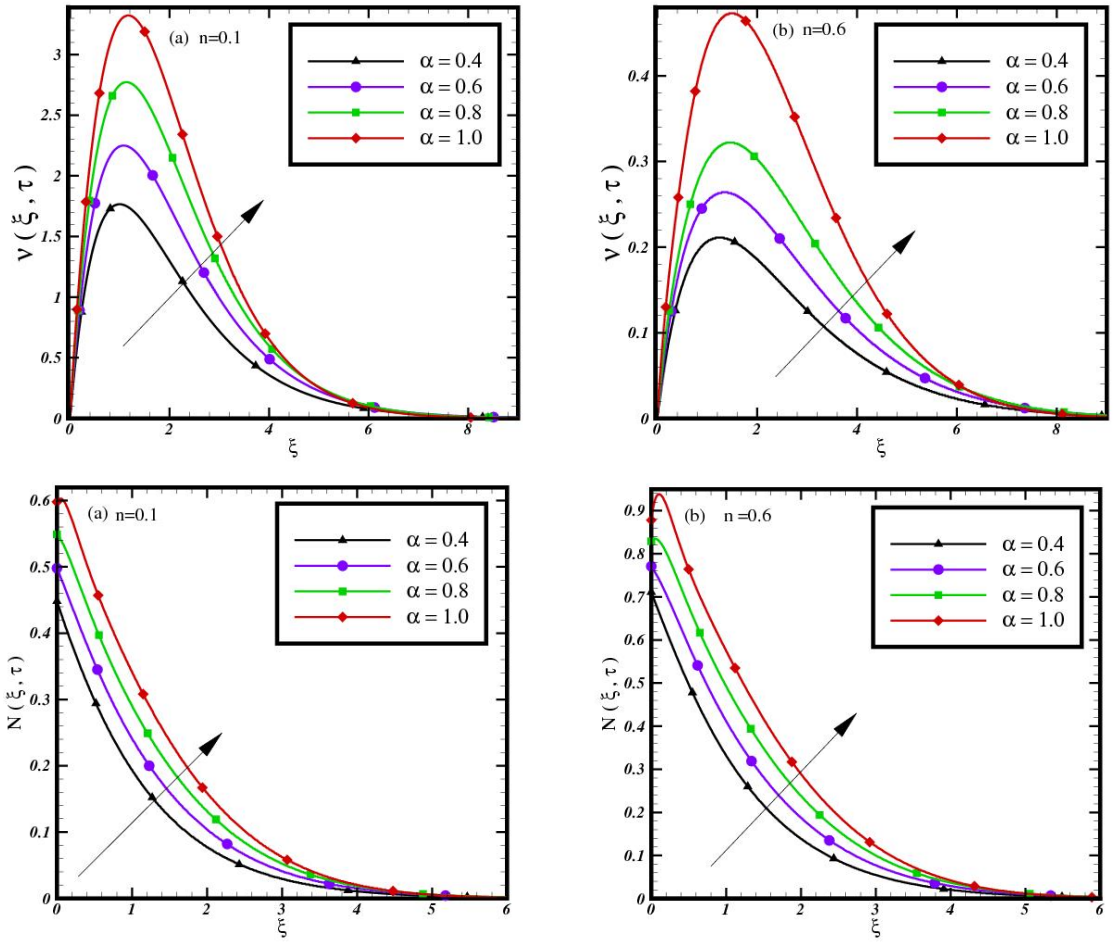

Figure 7. Velocity and microrotation profiles against ξ for different values of n (a) $n=0.1$ and (b) $n=0.6$, where $\tau=3$, $\beta=0.2$, $\eta=1.5$, $Gr=10$, Pr$=10$, $n=0.1$, $R=2$, and $\omega\tau=\pi/2$.

Figure 8(a), (b) exhibits the influence of R on velocity and microrotation. Both flow characteristics demonstrate significant enhancement as R increases. This promoting effect stems from modified thermal transport mechanisms. Higher R values indicate a stronger radiative heat transfer contribution. This improves thermal energy penetration into the fluid layer. Consequently, fluid temperature rises more rapidly throughout the domain. The enhanced heating strengthens buoyancy forces significantly. This accelerates fluid motion through intensified natural convection. Meanwhile, the increased flow velocity generates greater shear rates. These elevated shear rates excite stronger microrotation effects. Additionally, radiation provides nonlocal energy transfer mechanisms. This further activates rotational degrees of freedom in the fluid.

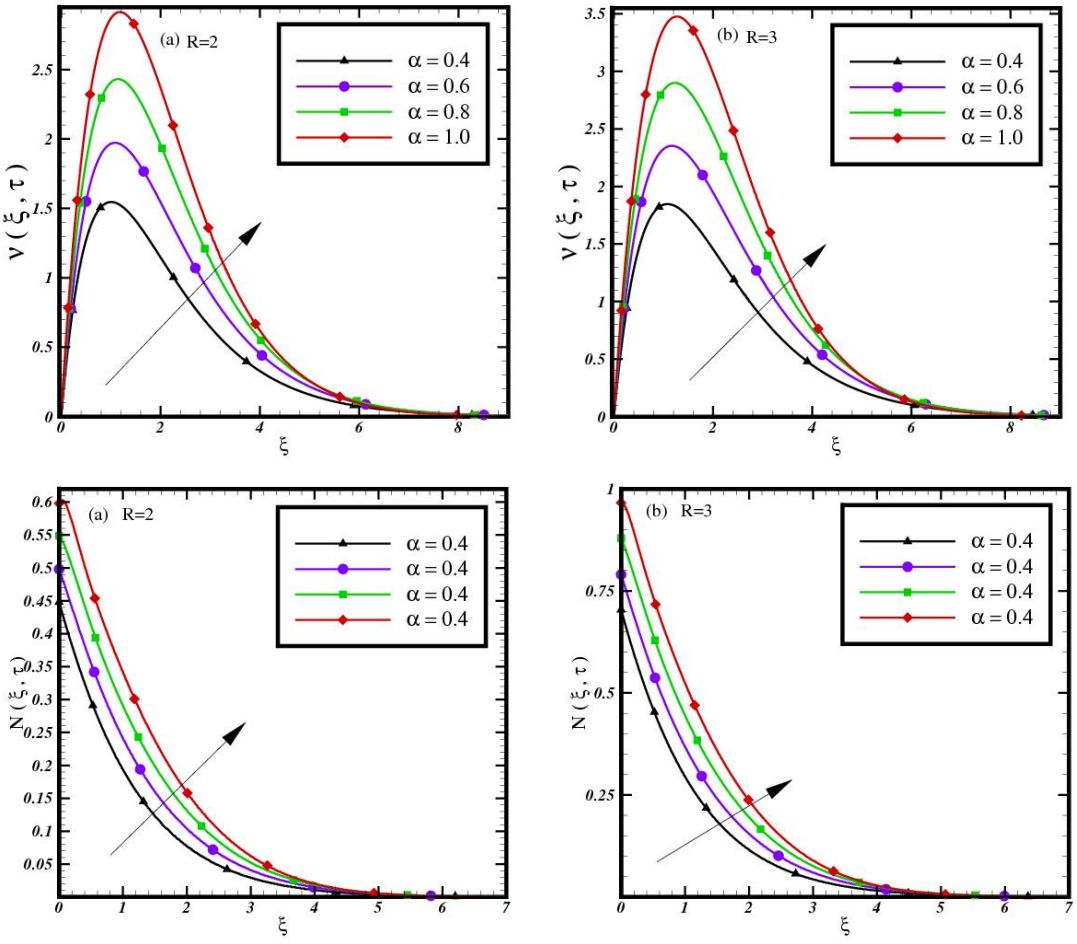

Figure 8. Velocity and microrotation profiles against ξ for different values of R (a) $R=2$ and (b) $R=3$, where $\tau=3$, $\beta=0.2$, $\eta=1.5$, $Gr=10$, $\mathrm{Pr}=10$, $n=0.1$, $R=2$, and $\omega\tau=\pi/2$.

Figure 9(a), (b) displays the influence of $\omega\tau$ on velocity and microrotation. Both hydrodynamic properties show increasing magnitudes with higher $\omega\tau$ values. This enhancement results from improved synchronization between plate motion and fluid response. Larger phase angles create constructive interference in the flow domain. This amplifies resonance effects within the boundary layer. Consequently, momentum transfer from the boundary becomes more efficient. Meanwhile, the intensified fluid motion generates stronger vorticity patterns. These patterns directly excite micro-rotational components in the fluid. Thus, both translation and rotation mechanisms gain energy. Moreover, the system shows a stronger dynamic response under phase-synchronized excitation.

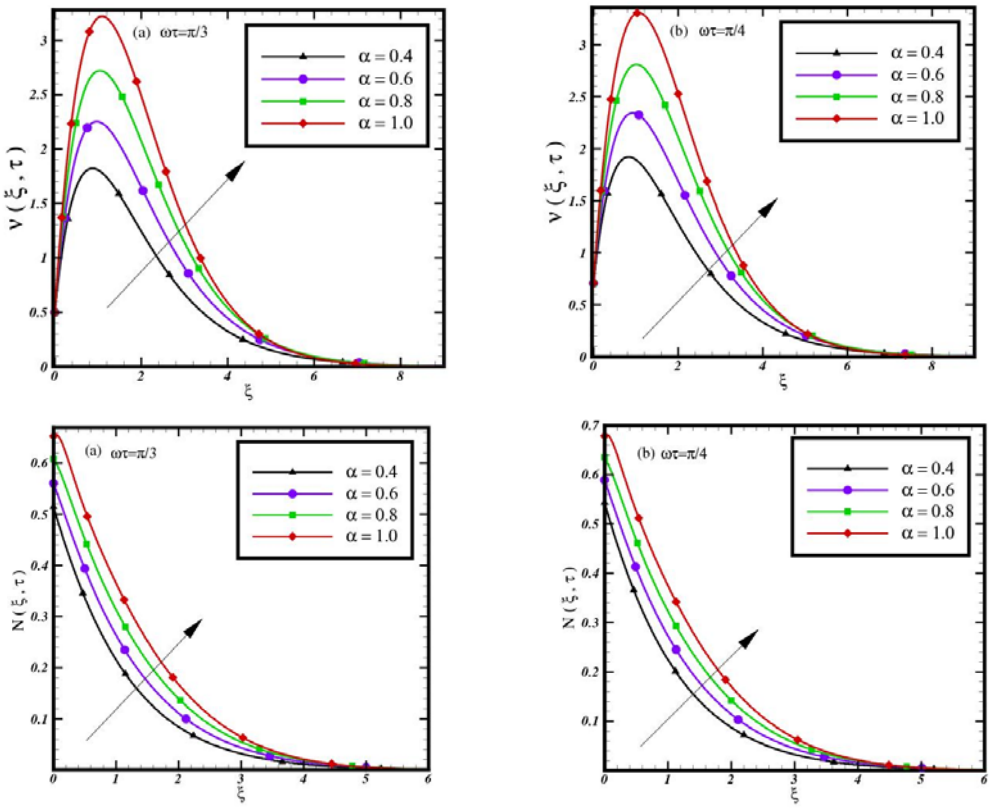

Figure 9. Velocity and microrotation profiles against ξ for different values of $\omega\tau$ (a) $\omega\tau=\pi/3$ and (b) $\omega\tau=\pi/4$, where $\tau=3$, $\beta=0.2$, $\eta=1.5$, $Gr=10$, Pr$=10$, $n=0.1$, and $R=2$.

Figure 10 (a),(b) presents the temperature distribution for increasing τ. Temperature levels show progressive elevation throughout the fluid domain. This occurs due to sustained thermal energy input from the boundary. Longer duration allows deeper heat penetration into the fluid. Meanwhile, thermal diffusion and radiation mechanisms operate continuously. Consequently, the thermal boundary layer thickens with time. Moreover, radiation facilitates deeper energy penetration through volumetric heating. Thus, internal fluid layers experience temperature rises even away from the boundary.

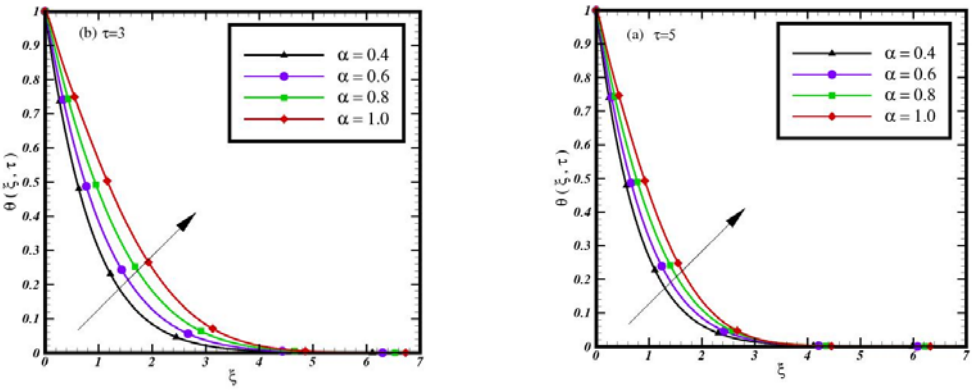

Figure 10. Temperature profile against ξ for different values of τ (a) $\tau=3$ and (b) $\tau=5$ where $\tau=3$ $R=2$ and Pr=10, and $R=2$.

Figure 11(a), (b) demonstrates the influence of radiation parameter R on temperature distribution. Temperature profiles show significant enhancement with increasing R values. This occurs through two primary radiation mechanisms. First, higher R strengthens radiative thermal conductivity. This enables more efficient deep-layer energy transport. Second, it augments volumetric absorption of thermal energy. Radiation bypasses conductive transport limitations. Consequently, heat penetrates beyond conventional boundary layers. The thermal penetration depth increases substantially.

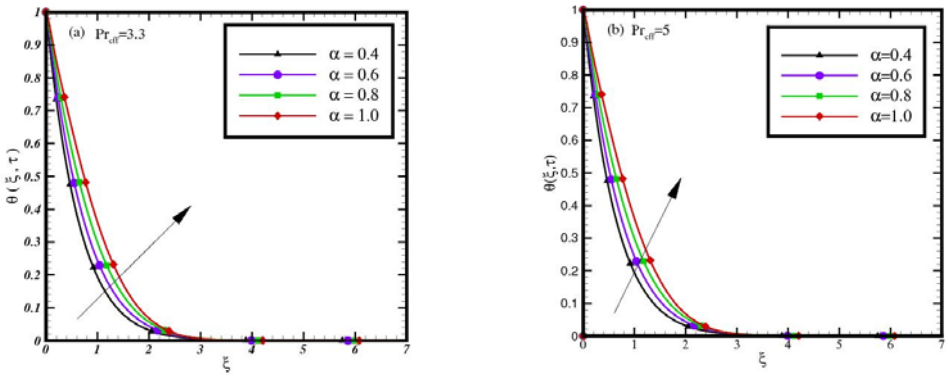

Figure 11. Temperature profile against ξ for different values of Pr_{eff} (a) Pr_{eff} =3.3 and (b) Pr_{eff} =5 where τ=*3,* and R=2.

Figure 12 (a),(b) analyzes the influence of Pr_{eff} on temperature distribution. Temperature profiles show a significant decrease with increasing Pr_{eff} values. This suppression results from altered thermal transport properties. Higher Pr_{eff} indicates reduced thermal diffusivity relative to momentum diffusivity. This restricts heat propagation away from the heated boundary. Consequently, thermal energy becomes concentrated near the wall region. Meanwhile, the impaired thermal diffusion creates steeper temperature gradients. Additionally, the thermal boundary layer thickness reduces substantially. This confinement limits thermal penetration into the fluid domain. Furthermore, the fractional model captures how Pr_{eff} interacts with memory effects.

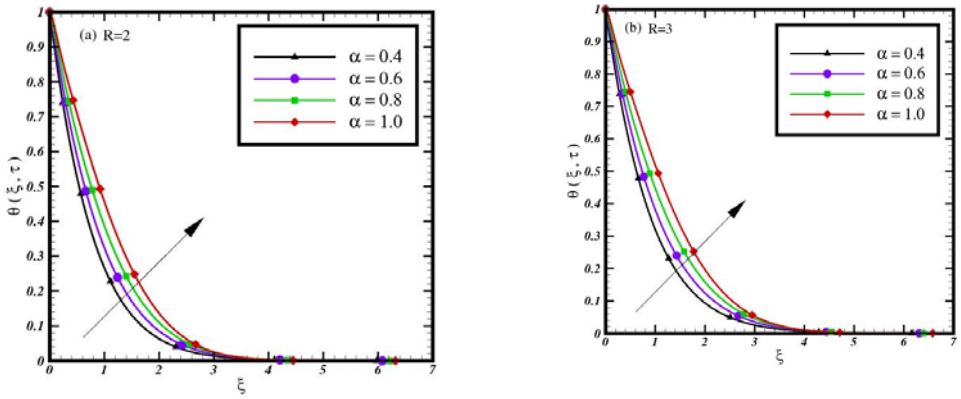

Figure 12. Temperature profile against ξ for different values of R (a) *R=2* and (b) *R=3* where τ=3, Pr_{eff} =3.3.

Table 1 presents a systematic numerical investigation of skin friction (C_f) variations across nine key physical parameters. The analysis reveals distinct parametric influences on wall shear stress characteristics in fractional micropolar fluid flow. The C_f demonstrates a strong positive correlation with α through memory-enhanced boundary acceleration mechanisms. With increasing α, the skin friction increases, approaching the classical case without memory effects. Lower α capture the memory effect, which reduces the wall shear stress compared to the classical model. Higher Gr intensifies C_f by strengthening thermal buoyancy effects and convective momentum transfer. The R increases C_f through improved thermal penetration and enhanced energy absorption capabilities. Furthermore, τ shows a progressively increasing relationship with C_f. Extended temporal duration allows deeper momentum diffusion and boundary layer development. The $\omega\tau$ enhances C_f through optimized resonant synchronization with plate oscillations. These factors collectively promote greater wall shear stress generation through different physical mechanisms. Conversely, C_f decreases with several other parameters. The n reduces shear stress by diverting energy from translational to rotational motion modes. Pr_{eff} diminishes C_f by suppressing thermal boundary layer growth and buoyancy-driven flow components. β demonstrates a significant inverse relationship through enhanced vortex viscosity effects that dampen near-wall velocities. The η shows comparatively minimal influence on C_f characteristics. This indicates its primary effect manifests in rotational dynamics rather than translational boundary layer development. The parameter interactions reveal complex nonlinear behavior in certain combinations, particularly between α and β where memory effects partially counteract microstructural resistance.

Table 1. Influence of pertinent parameters on skin friction.

α	β	η	Gr	Pr_{eff}	n	R	τ	$\omega\tau$	C_f
0.4	0.2	1.5	10	3.3	0.1	2	3	π/3	16.9
0.6	0.2	1.5	10	3.3	0.1	2	3	π/3	19.9
1	0.2	1.5	10	3.3	0.1	2	3	π/3	26.651
0.4	**0.6**	1.5	10	3.3	0.1	2	3	π/3	15.7
0.4	0.2	**2.5**	10	3.3	0.1	2	3	π/3	16.8
0.4	0.2	1.5	**15**	3.3	0.1	2	3	π/3	25.7
0.4	0.2	1.5	10	**5**	0.1	2	3	π/3	14.5
0.4	0.2	1.5	10	3.3	**0.3**	2	3	π/3	16.2
0.4	0.2	1.5	10	3.3	0.1	**3**	3	π/3	18.7
0.4	0.2	1.5	10	3.3	0.1	2	**5**	π/3	18.8
0.4	0.2	1.5	10	3.3	0.1	2	3	**π/2**	18.6

Table 2 systematically examines wall couple stress sensitivity to nine physical parameters. The dimensionless couple stress (C_m)shows distinct response patterns to various influences. This stress component represents rotational resistance at the boundary surface. The C_m increases significantly with α. Memory effects enhance micro-rotational gradients near the wall. Higher Gr amplifies C_m through buoyancy-driven flow intensification. The n strongly increases rotational stresses through

enhanced coupling between translation and rotation. The R elevates C_m by improving thermal energy transfer. The $\omega\tau$ increases C_m through resonant excitation of rotational modes. These parameters collectively promote greater micro-rotational resistance at the boundary. Conversely, C_m decreases with several parameters. The β reduces rotational stress through vortex viscosity dissipation. The η diminishes C_m by diffusing rotational momentum. The $\mathrm{Pr}_{\mathrm{eff}}$ lowers rotational stress by suppressing thermal effects on microstructure. The τ shows a reducing effect on C_m. Longer duration allows rotational energy dispersion away from the wall. This temporal behavior contrasts with its effect on C_f. Parameter interactions reveal interesting compensatory effects. For instance, high n with low β produces maximum rotational stress. Meanwhile, high η with high Pr_{eff} shows minimal C_m values.

Table 2. Influence of pertinent parameter on wall couple stress.

α	β	η	Gr	Pr_{eff}	n	R	τ	$\omega\tau$	C_W
0.4	0.2	1.5	10	3.3	0.1	2	3	π/3	0.68
0.6	0.2	1.5	10	3.3	0.1	2	3	π/3	0.56
0.4	**0.6**	1.5	10	3.3	0.1	2	3	π/3	0.28
0.4	0.2	**2.5**	10	3.3	0.1	2	3	π/3	0.62
0.4	0.2	1.5	**15**	3.3	0.1	2	3	π/3	1.04
0.4	0.2	1.5	10	**5**	0.1	2	3	π/3	0.37
0.4	0.2	1.5	10	3.3	**0.3**	2	3	π/3	1.11
0.4	0.2	1.5	10	10	0.1	**3**	3	π/3	1.07
0.4	0.2	1.5	10	10	0.1	2	**5**	π/3	0.6
0.4	0.2	1.5	10	10	0.1	2	3	**π/2**	0.57

Table 3 systematically examines how the Nusselt number (Nu) responds to α, Pr_{eff} and τ. The Nu decreases with increasing α, indicating reduced heat transfer as the system approaches the classical model. Lower α enhances the thermal response due to memory effects. The results show Nu increases with higher Pr_{eff} values. This occurs because greater Pr_{eff} enhances thermal conductivity relative to viscosity. Consequently, heat transfer rates improve significantly at the boundary. Meanwhile, Nu decreases with advancing τ. Longer duration allows thermal boundary layer development. This thickening layer reduces temperature gradients at the wall. Thus, heat transfer efficiency gradually diminishes over time.

Table 3. Influence of pertinent parameters on Nusselt number.

α	Pr	R	τ	Nu
0.4	10	2	3	2.4
0.6	10	2	3	1.8
1	10	2	3	0.60
0.4	**15**	2	3	2.9
0.4	10	**3**	3	3.1

The bold numbers in all tables indicate parameter variations. These highlight deviations from the baseline configuration in the first row. Furthermore, they facilitate quick comparison of parametric influences across different outputs.

6. Conclusions

This study successfully develops a generalized fractional model for analyzing convection flow of a micropolar fluid over an oscillating vertical plate, incorporating thermal radiation and memory effects via Caputo fractional derivatives. Exact analytical solutions for velocity, microrotation, and temperature fields are derived using the Laplace transform method and expressed in terms of Wright functions, which inherently preserve memory effects and provide a strong mathematical framework for capturing nonlocal dynamics. The solutions generalize classical fluid models by reducing to limiting cases such as Stokes' first problem and fractional viscous fluids, validating the consistency and versatility of the proposed approach.

Parametric analysis reveals that α significantly enhances velocity, microrotation, and temperature profiles due to memory-driven acceleration and thermal accumulation. The $\omega\tau$ amplifies microrotation magnitudes through resonant coupling with oscillatory boundary motion, while τ promotes thermal diffusion and boundary layer growth. Conversely, β suppresses flow and rotation by increasing microstructural resistance, and η exhibits dual behavior: enhancing velocity while dampening microrotation due to energy redistribution between translational and rotational modes. The R consistently elevates temperature and flow profiles by improving thermal penetration, whereas Pr_{eff} attenuates temperature distributions through reduced thermal diffusivity.

Quantitative results demonstrate that skin friction intensifies with higher α and Gr, but diminishes with increasing β and Pr_{eff}. Wall couple stress rises with α, Gr, and n, but declines with β and η. The Nusselt number increases with Pr_{eff} due to sharper thermal gradients but decreases with time as boundary layers stabilize.

This work unified fractional calculus, micropolar theory, and oscillatory boundary conditions to address memory-dependent phenomena in fluids, offering benchmark solutions for applications in microfluidics, geothermal systems, and biomedical engineering. Future studies could extend this model to include mass transfer, chemical reactions, or alternative fractional operators to explore broader thermodynamic and hydrodynamic interactions

7. Future recommendations

Although the present study focuses on unidirectional, one-dimensional flow, it can be extended in several directions. Future research may consider other non-Newtonian fluids, such as second-grade, third-grade, Maxwell, Oldroyd-B, and Berger fluids. Additionally, investigations could include nano and hybrid nanofluids, as well as new fractional operators, such as Caputo-Fabrizio and Atangana-Baleanu operators. Moreover, two and three-dimensional flow configurations can be explored to provide a more comprehensive understanding.

8. Nomenclature

C_p	Specific heat
$D^{\alpha}(.)$	Caputo fractional derivative
k_1	Thermal conductivity
k_2	Mean absorption
j	Microinertia
N	Micro rotation
n	Microgyration
q_r	Radiative heat flux
T	Fluid temperature
T_W	Plate temperature
T_W	Ambient temperature
u	x-component of velocity
v	Dimensionless velocity
t	Time
Gr	Grashof number
Pr	Prandtl number
R	Radiation parameter
y	y-coordinate
Greek letters	
α	Fractional order
α_1	Vertex viscosity
β	Micropolar parameter
β_T	Thermal expansion
γ	Spin gradient
ρ	Density of the fluid
μ	Dynamic viscosity
τ	Dimensionless time
ξ	Dimensionless y-coordinate
σ_1	Stefan-Boltzmann constant
ω	Frequency of oscillation
η	Dimensionless spin gradient
θ	Dimensionless temperature

Use of Generative-AI tools declaration

The author declares he has not used Artificial Intelligence (AI) tools in the creation of this article.

Conflict of interest

The authors declare no competing financial interests.

References

1. I. Podlubny, *Fractional differential equations: An introduction to fractional derivatives, fractional differential equations, to methods of their solution and some of their applications*, Elsevier, 1998.
2. V. V. Kulish, J. L. Lage, Application of fractional calculus to fluid mechanics, *J. Fluid. Eng.*, **124** (2002), 803–806. https://doi.org/10.1115/1.1478062
3. R. L. Magin, Fractional calculus in bioengineering: A tool to model complex dynamics, IEEE, 2012, 464–469. https://doi.org/10.1109/CarpathianCC.2012.6228688
4. K. Oldham, J. Spanier, *The fractional calculus theory and applications of differentiation and integration to arbitrary order*, Elsevier, 1974.
5. M. D. Ortigueira, J. A. T. Machado, Fractional signal processing and applications, *Signal Proc.,* **83** (2003), 2285–2286. https://doi.org/10.1016/S0165-1684(03)00181-6
6. F. Mainardi, *Fractional calculus and waves in linear viscoelasticity: An introduction to mathematical models*, World Scientific, 2022.
7. R. Metzler, J. Klafter, The random walk's guide to anomalous diffusion: A fractional dynamics approach, *Phys. Rep.,* **339** (2000), 1–77. https://doi.org/10.1016/S0370-1573(00)00070-3
8. T. M. Atanackovic, S. Pilipovic, B. Stankovic, D. Zorica, *Fractional calculus with applications in mechanics: vibrations and diffusion processes*, John Wiley & Sons, 2014. https://doi.org/10.1002/9781118577530
9. G. E. Karniadakis, I. G. Kevrekidis, L. Lu, P. Perdikaris, S. F. Wang, L. Yang, Physics-informed machine learning, *Nat. Rev. Phys.,* **3** (2021), 422–440. https://doi.org/10.1038/s42254-021-00314-5
10. C. H. R. Friedrich, Relaxation and retardation functions of the Maxwell model with fractional derivatives, *Rheol. Acta,* **30** (1991), 151–158. https://doi.org/10.1007/BF01134604
11. W. C. Tan, W. X. Pan, M. Y. Xu, A note on unsteady flows of a viscoelastic fluid with the fractional Maxwell model between two parallel plates, *Int. J. Non-Lin. Mech.*, **38** (2003), 645–650. https://doi.org/10.1016/S0020-7462(01)00121-4
12. N. Makris, M. C. Constantinou, Fractional-derivative maxwell model for viscous dampers, *J. Struct. Eng.,* **117** (1991), 2708–2724. https://doi.org/10.1061/(ASCE)0733-9445(1991)117:9(2708)
13. A. A. Zafar, C. Fetecau, I. A. Mirza, On the flow of Oldroyd-B fluids with fractional derivatives over a plate that applies shear to the fluid, *arXiv:14084526,* 2014.
14. A. W. Shaikh, G. Q. Memon, Z. A. Kalhoro, S. Muttaqi, A. Soomro, U. A. Rind, Starting flows for a fractional Oldroyd-B fluid between two coaxial cylinders, *Sindh Univ. Res. J.-SURJ (Sci. Ser.)*, 2014, 46.
15. P. Kumar, Revolutionizing heat transfer and fluid flow models: Fractional calculus and non-newtonian dynamics meet advanced numerical methods, *Commun. Appl. Nonlinear Anal.* **32** (2024), 471–489.
16. S. Riaz, M. S. Anwar, A. Jamil, T. Muhammad, Advanced fractional model for predicting MHD yield stress fluid flow with boundary effects, *Nonlinear Dyn.,* **113** (2025), 1–17. https://doi.org/10.1007/s11071-025-11018-1
17. M. Irfan, M. S. Anwar, S. S. Abas, Z. Hussain, M. Khan, Thermal behavior and efficiency enhancement of CuO-Al_2O_3 hybrid nanofluids using fractional calculus, *J. Therm. Anal. Calorim.,* **150** (2025), 2181–2194. https://doi.org/10.1007/s10973-024-13822-0
18. W. Tan, F. Xian, L. Wei, An exact solution of unsteady Couette flow of generalized second grade fluid, *Chinese Sci. Bull.*, **47** (2002), 1783–1785. https://doi.org/10.1360/02tb9389

19. M. A. Imran, I. Khan, M. Ahmad, N. A. Shah, M. Nazar, Heat and mass transport of differential type fluid with non-integer order time-fractional Caputo derivatives, *J. Mol. Liq.,* **229** (2017), 67–75. https://doi.org/10.1016/j.molliq.2016.11.095
20. M. Kamran, M. Imran, M. Athar, Exact solutions for the unsteady rotational flow of a generalized second grade fluid through a circular cylinder, *Nonlinear Anal.-Model.*, **15** (2010), 437–444. https://doi.org/10.15388/NA.15.4.14315
21. A. Shakeel, S. Ahmad, H. Khan, D. Vieru, Solutions with Wright functions for time fractional convection flow near a heated vertical plate, *Adv. Differ. Equ.*, **1** (2016), 51. https://doi.org/10.1186/s13662-016-0775-9
22. I. Khan, N. A. Shah, D. Vieru, Unsteady flow of generalized Casson fluid with fractional derivative due to an infinite plate, *Eur. Phys. J. Plus,* **131** (2016), 181. https://doi.org/10.1140/epjp/i2016-16181-8
23. N. A. Shah, I. Khan, Heat transfer analysis in a second grade fluid over and oscillating vertical plate using fractional Caputo–Fabrizio derivatives, *Eur. Phys. J. C*, **76** (2016), 362. https://doi.org/10.1140/epjc/s10052-016-4209-3
24. F. Ali, S. A. A. Jan, I. Khan, M. Gohar, N. A.Sheikh, Solutions with special functions for time fractional free convection flow of Brinkman-type fluid, *Eur. Phys. J. Plus,* **131** (2016), 310. https://doi.org/10.1140/epjp/i2016-16310-5
25. D. Vieru, C. Fetecau, C. Fetecau, Time-fractional free convection flow near a vertical plate with Newtonian heating and mass diffusion, *Therm. Sci.,* **19** (2015), 85–98. https://doi.org/10.2298/TSCI15S1S85V
26. I. Mahariq, H. A. Ghazwani, M. A. Shah, Enhancing heat and mass transfer in MHD tetra hybrid nanofluid on solar collector plate through fractal operator analysis, *Res. Eng.,* **24** (2024), 103163. https://doi.org/10.1016/j.rineng.2024.103163
27. Y. Sokolovskyy, T. Samotii, Adaptive fractional neural algorithm for modeling heat-and-mass transfer, *Comput. Des. Syst. Theory Pract.*, **6** (2024), 139–153. https://doi.org/10.23939/cds2024.03.139
28. A. C. Eringen, Theory of micropolar fluids, *J. Math. Mech.*, 1966, 1–18. https://doi.org/10.1512/iumj.1967.16.16001
29. T. Ariman, A. S. Cakmak, Some basic viscous flows in micropolar fluids, *Rheol. Acta,* **7** (1968), 236–242. https://doi.org/10.1007/BF01985784
30. M. A. Seddeek, S. N. Odda, M. Y. Akl, M. S. Abdelmeguid, Analytical solution for the effect of radiation on flow of a magneto-micropolar fluid past a continuously moving plate with suction and blowing, *Comput. Mat. Sci.,* **45** (2009), 423–428. https://doi.org/10.1016/j.commatsci.2008.11.001
31. H. H. Sherief, M. S. Faltas, E. A. Ashmawy, Exact solution for the unsteady flow of a semi-infinite micropolar fluid, *Acta Mech. Sinica,* **27** (2011), 354–359. https://doi.org/10.1007/s10409-011-0452-4
32. A. Khalid, I. Khan, A. Khan, S. Shafie, Conjugate transfer of heat and mass in unsteady flow of a micropolar fluid with wall couple stress, *AIP Adv.,* **5** (2015), 127125. https://doi.org/10.1063/1.4938551
33. A. Hussanan, M. Z. Salleh, I. Khan, R. M. Tahar, Heat and mass transfer in a micropolar fluid with Newtonian heating: An exact analysis, *Neural Comput. Appl.,* **29** (2018), 59–67. https://doi.org/10.1007/s00521-016-2516-0
34. A. Kumar, P. K. Yadav, Heat and mass transfer analysis of non-miscible couple stress and micropolar fluids flow through a porous saturated channel, *ZAMM,* **104** (2024), e202300635. https://doi.org/10.1002/zamm.202300635

35. H. R. Patel, S. D. Patel, Heat and mass transfer in mixed convection MHD micropolar fluid flow due to non-linear stretched sheet in porous medium with non-uniform heat generation and absorption, *Waves Random Complex,* **35** (2025), 2551–2581. https://doi.org/10.1080/17455030.2022.2044542
36. A. Imran, H. Alzubadi, M. R. Ali, A computation analysis with heat and mass transfer for micropolar nanofluid in ciliated microchannel: With application in the ductus efferentes, *Heliyon,* **10** (2024), e39018. https://doi.org/10.1016/j.heliyon.2024.e39018
37. N. A. Sheikh, F. Ali, I. Khan, M. Saqib, A. Khan, MHD flow of micropolar fluid over an oscillating vertical plate embedded in porous media with constant temperature and concentration, *Math. Probl. Eng.,* **2017** (2017), 9402964. https://doi.org/10.1155/2017/9402964

AIMS Press